

RESEARCH LETTER

10.1002/2017GL075506

Key Points:

- Slowly slipping faults have the potential to enhance reservoir stimulation in extremely low permeability shale reservoirs
- Permeability recovery most likely occurs on a smooth fault with high calcite content when effective stress returns to the initial value
- Permeability evolution of slowly slipping faults depends on shale mineralogy, fault characteristics, and stress conditions

Supporting Information:

- Supporting Information S1

Correspondence to:

W. Wu,
wu.wei@ntu.edu.sg

Citation:

Wu, W., Reece, J. S., Gensterblum, Y., & Zoback, M. D. (2017). Permeability evolution of slowly slipping faults in shale reservoirs. *Geophysical Research Letters*, 44, 11,368–11,375. <https://doi.org/10.1002/2017GL075506>

Received 1 JUN 2017

Accepted 27 OCT 2017

Accepted article online 6 NOV 2017

Published online 27 NOV 2017

Permeability Evolution of Slowly Slipping Faults in Shale Reservoirs

Wei Wu¹ , Julia S. Reece² , Yves Gensterblum³, and Mark D. Zoback⁴ 

¹School of Civil and Environmental Engineering, Nanyang Technological University, Singapore, ²Department of Geology and Geophysics, Texas A&M University, College Station, TX, USA, ³International Academy, RWTH Aachen University, Aachen, Germany, ⁴Department of Geophysics, Stanford University, Stanford, CA, USA

Abstract Slow slip on preexisting faults during hydraulic fracturing is a process that significantly influences shale gas production in extremely low permeability “shale” (unconventional) reservoirs. We experimentally examined the impacts of mineralogy, surface roughness, and effective stress on permeability evolution of slowly slipping faults in Eagle Ford shale samples. Our results show that fault permeability decreases with slip at higher effective stress but increases with slip at lower effective stress. The permeabilities of saw cut faults fully recover after cycling effective stress from 2.5 to 17.5 to 2.5 MPa and increase with slip at constant effective stress due to asperity damage and dilation associated with slip. However, the permeabilities of natural faults only partially recover after cycling effective stress returns to 2.5 MPa and decrease with slip due to produced gouge blocking fluid flow pathways. Our results suggest that slowly slipping faults have the potential to enhance reservoir stimulation in extremely low permeability reservoirs.

1. Introduction

Advances in drilling and fracturing technologies, like horizontal drilling and multistage hydraulic fracturing, have enabled substantial growth in shale gas production. These technologies not only create extensive permeable fracture networks in unconventional reservoirs but also have the potential to activate preexisting fractures and faults. Slow slip, known as the dominant mode of fault activation, is expected to be controlled by the rate strengthening behavior (Kohli & Zoback, 2013) and could potentially contribute to reservoir stimulation (Zoback et al., 2012). Das and Zoback (2013) revealed that the recently recognized long-period long-duration events are associated with slow slip on relatively large faults. Several studies have shown that fault permeability changes as a result of slow slip, but the mechanism remains poorly understood. The permeability of mechanically split faults in Kimmeridge shale samples using a direct shear apparatus was dependent on the normal load (Gutierrez et al., 2000). In this case, the permeability increased with slip at low normal loads due to gouge formation and dilation but decreased with slip at high normal loads due to gouge compaction. Reece et al. (2014) measured fault permeability in Haynesville shale samples before and after slow slip using a conventional triaxial apparatus. At an effective stress of 13.0 MPa, the permeabilities of saw cut and natural faults decreased with a few millimeters of slip by a few orders of magnitude. Gensterblum and Zoback (2015) used the same apparatus at 3.5 MPa effective stress and observed that the permeability of a saw cut fault in a clay-rich Haynesville shale sample significantly declined after slow slip, whereas the permeability of a saw cut fault in a calcite-rich Eagle Ford shale sample slightly increased. Fang et al. (2017) also found that permeability evolution of sheared faults was dependent on the mineral composition of shale samples and the competition between sealing wear products and slip-associated dilation. Permeability enhancement has also been observed in experimentally produced faults in other rocks. The permeability of an extensional fault in a granite sample increased with larger shear displacement and lower normal loads (Lee & Cho, 2002).

We conducted shear flow experiments on saw cut and natural faults in Eagle Ford shale samples to investigate the impacts of mineralogy, surface roughness, and effective stress on permeability evolution of slowly slipping faults. Understanding these relationships will help us effectively improve fracturing technologies and ultimately enhance reservoir stimulation in extremely low permeability reservoirs.

2. Experimental Setup and Procedures

The Eagle Ford shale is a Late Cretaceous-age sedimentary rock sourced from South Texas with highly variable composition, low porosity (5%–7%) (Sone & Zoback, 2013a), high strength (uniaxial compressive

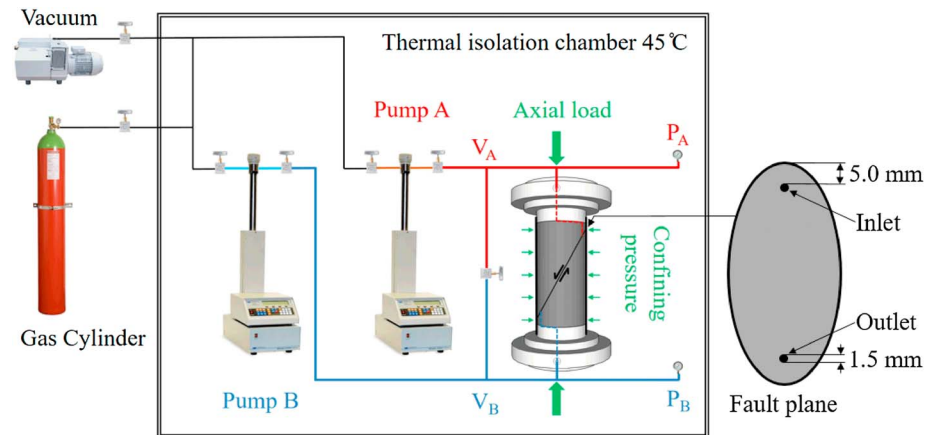


Figure 1. Schematic diagram of the experimental setup. Pumps A and B control the upstream and downstream pressures, respectively.

strength >120 MPa) (Sone & Zoback, 2013b), and very low permeability parallel to bedding planes (3 nD–12 μD) (Heller et al., 2014).

As we expected shale mineralogy to be one of several factors significantly influencing fault permeability, we selected two Eagle Ford shale blocks based on the results of X-ray powder diffraction analyses. One clay-rich shale block has a mineral composition of 26% clay, 43% calcite, 19% quartz, 2% feldspar, 5% pyrite, and 5% total organic carbon (TOC) content, and the other calcite-rich shale block contains 86% calcite, 9% quartz, 1% pyrite, and 4% TOC. We drilled cylindrical core plugs from both clay-rich and calcite-rich blocks. The 25.4 mm diameter core plugs were saw cut and surface ground to a length of 50.8 mm. A saw cut fault was manufactured by cutting a core sample at 30° to the core axis and polishing it using an ultrafine sandpaper with 16 μm particle size (600 grit). A natural fault was prepared by coring a cylindrical sample from a selected block with an open and unfilled fault oriented at 30° to the vertical direction. We then drilled 1.5 mm diameter boreholes parallel to the core axis at both ends of each sample to facilitate fluid flow from the coreholders to the fault plane (Figure 1). Four fault types with different combinations of shale mineralogy and fault surface topography were prepared: (1) saw cut fault in a clay-rich sample, (2) saw cut fault in a calcite-rich sample, (3) natural fault in a clay-rich sample, and (4) natural fault in a calcite-rich sample.

We performed shear flow experiments on prepared faults in shale samples using a GCTS triaxial testing system. Each sample was jacketed using a 0.75 mm heat-shrink Viton sleeve, which was then sealed on two steel coreholders using steel wires. The confining pressure was measured using a Heise DXD pressure transducer accurate to ±0.1% up to 68.9 MPa. The upstream and downstream pore pressures were controlled by the ISCO syringe pumps A and B, respectively. The pumps, which measure pressures with an accuracy of ±0.3% of the full scale and deliver pressures up to 68.9 MPa, were used to measure pore pressures and control flow rates. The experiments were conducted inside a thermally insulated chamber with a temperature control system maintained a constant temperature of 45°C (±0.2°C).

We used silicone oil as the confining fluid, compressed argon gas as the permeating fluid, the pressure pulse-decay technique to measure the permeabilities of relatively low permeability faults (e.g., saw cut faults), and the steady state flow technique for relatively high permeability faults (e.g., natural faults). The pressure pulse-decay technique (Brace et al., 1968) measures the differential pressure along the fault plane after a pressure step is achieved. The permeability based on the pressure pulse-decay technique, k_{pd} , is calculated as

$$k_{pd} = \frac{cL\mu}{AP_m(1/V_1 + 1/V_2)}, \tag{1}$$

where c is the slope of the natural logarithm of $(P_1 - P_2)$ plotted versus time, P_1 is the upstream pressure, P_2 is the downstream pressure, P_m is the average value of P_1 and P_2 , μ is the gas viscosity, L is the distance between the two drilled boreholes on the fault plane, A is the cross-sectional area of the fault plane, and V_1 and V_2 are the upstream and downstream reservoir volumes, respectively.

The steady state flow technique (Scheidtger, 1974) records the differential pressure along the fault plane at a constant flow rate, q , of $8.33 \times 10^{-7} \text{ m}^3/\text{s}$, which is sufficiently low to achieve steady state flow along the fault plane. The permeability based on the steady state flow technique, k_{ss} , is calculated as

$$k_{ss} = \frac{2qL\mu P_2}{A(P_1 + P_2)}. \quad (2)$$

For both permeability techniques, the exact flow pathways between the inlet and outlet boreholes and the cross-sectional areas of the fault planes, which depend on fault surface topography, are unknown. But for given faults under similar geometric condition and consistent surface preparation, we assume that both the length of flow pathways between the two boreholes and the cross-sectional area of the fault planes do not significantly vary and experience minor changes during 0.43 mm of the total slip displacement. Thus, we can compare relative permeabilities throughout the experiments.

We conducted two suites of shear flow experiments on prepared faults. In the “varying fault type” (VFT) suite of experiments, we performed four experiments, one for each fault type. In each experiment, we raised effective stress from 2.5 (Step 1) to 7.5 (Step 2) to 17.5 MPa (Step 3) and measured fault permeability at each effective stress. Returning effective stress to 2.5 MPa, we measured permeability before (Step 4) and after (Step 6) the slip event at a constant rate of 0.043 mm/min for 10 min (Step 5). We measured stress-dependent permeability at cyclic effective stresses to assess the effect of slow slip on fault intrinsic permeability and corresponding stress sensitivity coefficient. We repeated the above steps from Steps 6 to 9 to confirm the experimental reproducibility. Subsequently, we conducted three additional slip events (Steps 10, 12, and 14) at a constant effective stress of 2.5 MPa to observe the effect of continuing slip on permeability and measured permeability before and after each slip event (Steps 9, 11, 13, and 15).

The “varying effective stress” (VES) suite of experiments focused on the permeability of a saw cut fault in a clay-rich sample sheared three times at the same constant rate of 0.043 mm/min for 10 min but at varying effective stresses (2.5, 5.0, and 12.5 MPa). At the effective stress of 2.5 MPa, we measured fault permeability before (Step 1) and after (Step 3) the slip event (Step 2). Next, we repeated the slip event at 5.0 MPa effective stress in Step 5 and at 12.5 MPa effective stress in Step 8 and measured permeability before and after both slip events (Steps 4, 6, 7, and 9). After multiple slip events, we finally checked permeability recovery at 5.0 and 2.5 MPa effective stresses (Steps 10 and 11).

We also quantitatively imaged surface topographies of the four simulated faults from the VFT suite of shear flow experiments before and after all four slip events using a NextEngine 3-D laser scanner. Each sample was placed 15 to 23 cm away from the scanner in a sample holder, which tilted the sample toward the scanner so that the fault plane was vertical and as parallel to the scanner as possible. Each fault surface was imaged three times at a resolution of 0.127 mm, but only the best scan was used for analysis. The blue hole on each image indicates the inlet/outlet borehole. The zero datum was taken at the lowest topographic point in the borehole. Because of deep boreholes and small topographic changes in the case of the saw cut faults, the scale on the color bars for elevation (mm) and thickness (mm) was adjusted to clearly show topographic features. The thickness of the sheared layer for each sample was derived by subtracting the elevation after the shear flow experiment from that before the experiment and revealed size distribution of produced gouge in different faults.

3. Results

3.1. Topographic Changes of Fault Surfaces

Figure 2 shows that all four fault surfaces are fairly close to planar. The general topography is mirror imaged between corresponding top and bottom surfaces, so that a depression on one fault surface corresponds to a high on the other. Hence, we only show one fault surface in each case.

For saw cut faults, the surface topographies are quite even, and the thicknesses of the sheared layers in both clay-rich and calcite-rich samples are relatively uniform, indicating the formation of a well-sorted and fine-grained fault gouge. The maximum reduction of asperity elevation during slip is about 0.2 mm (Figures 2a and 2b). The initial surface roughness coefficients Z_2 (Tse & Cruden, 1979) of the saw cut faults in the clay-rich and calcite-rich samples are 0.07 and 0.10, respectively, and both are reduced to 0.04 after slip.

For natural faults, the topography extensively varies across the fault surface of the clay-rich sample (Figure 2c), whereas the change in topography across the fault surface of the calcite-rich sample is concentrated mainly

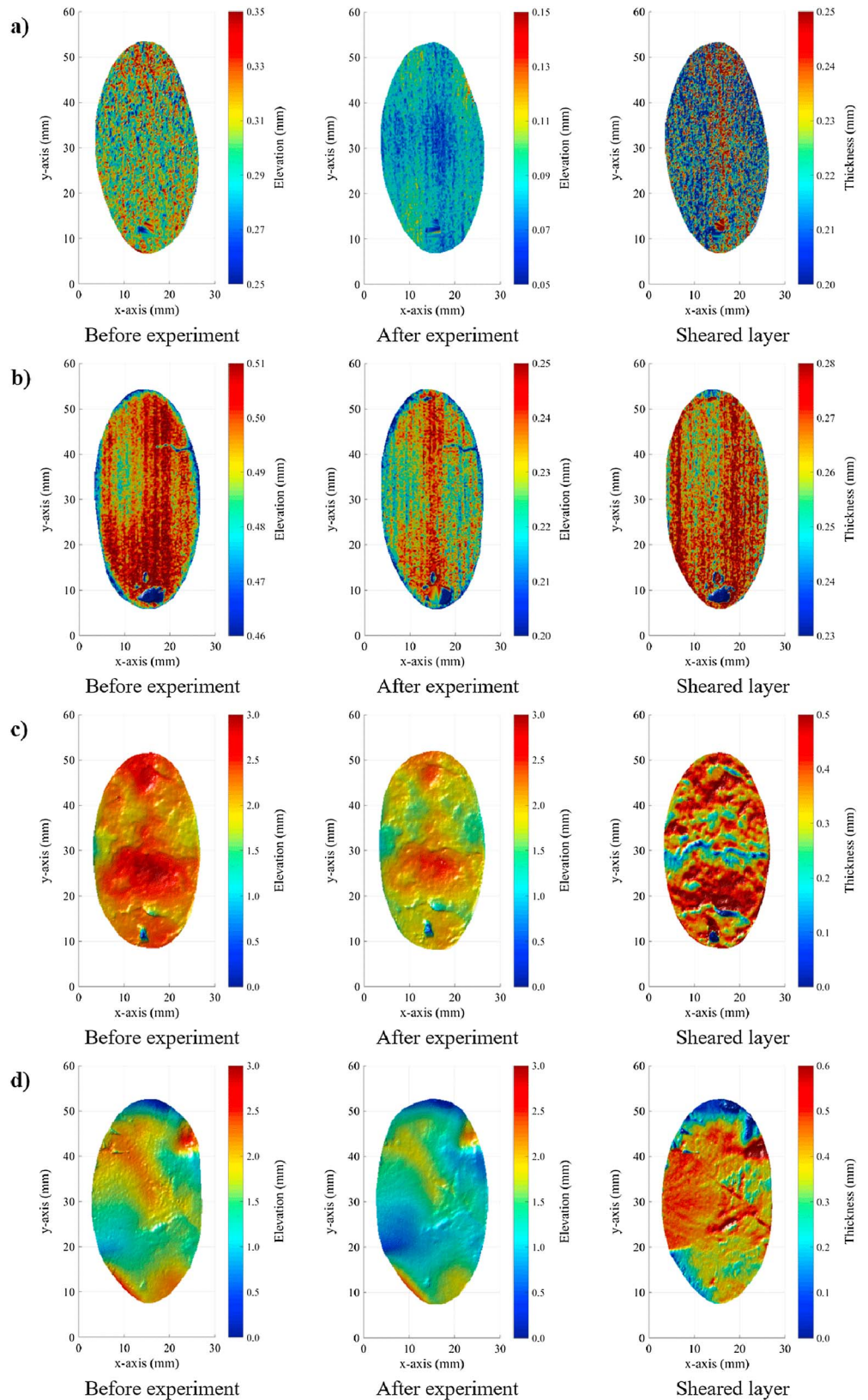


Figure 2. Topographic contours of four fault surfaces. (a) Saw cut surface of the clay-rich sample, (b) saw cut surface of the calcite-rich sample, (c) natural surface of the clay-rich sample, and (d) natural surface of the calcite-rich sample before (left column) and after (middle column) all four slip events. The right column shows the thickness of sheared layer in each case.

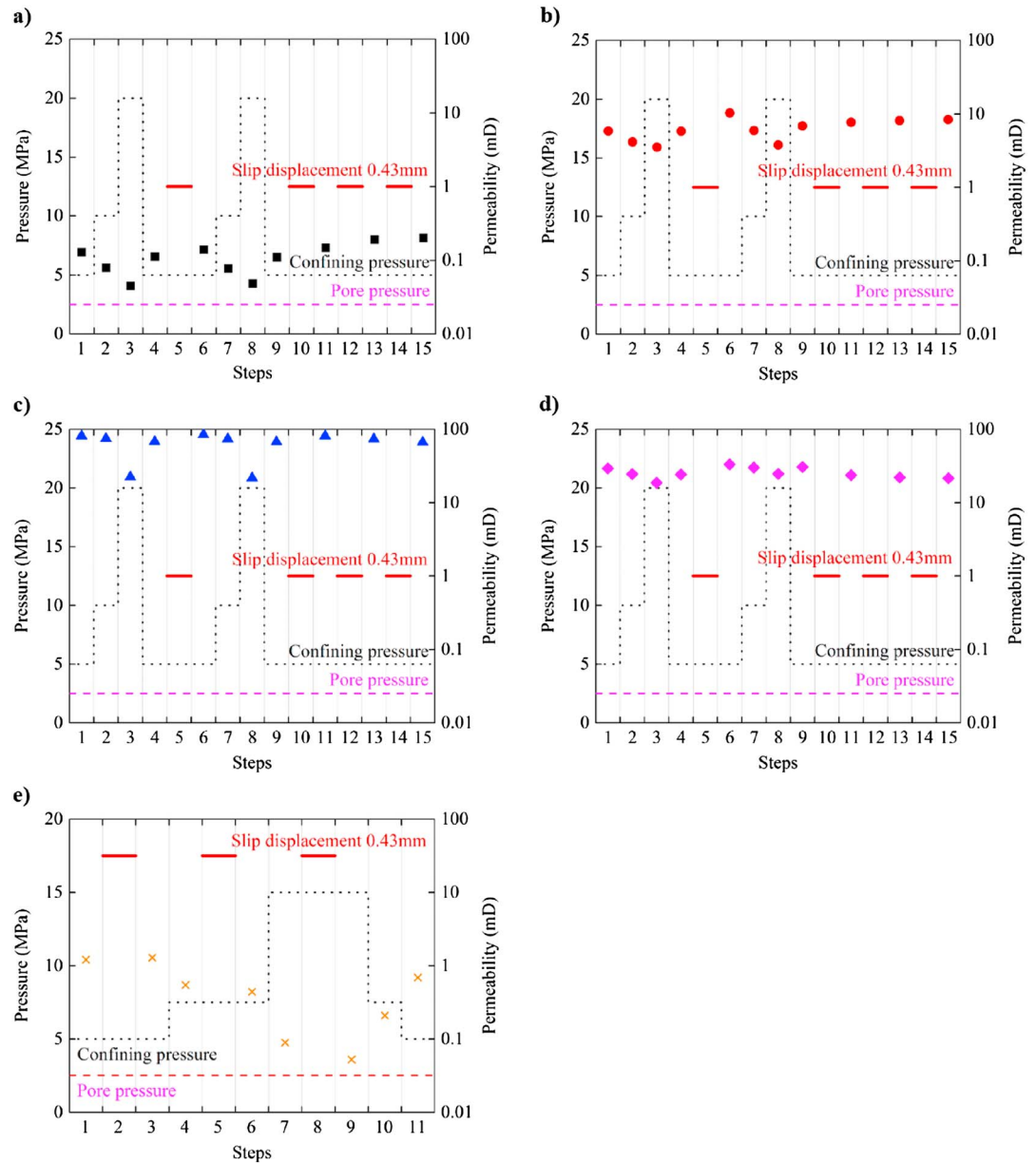


Figure 3. Permeability evolution of (a) saw cut fault in a clay-rich sample, (b) saw cut fault in a calcite-rich sample, (c) natural fault in a clay-rich sample, and (d) natural fault in a calcite-rich sample before and after slip at a constant effective stress, and (e) saw cut fault in a clay-rich sample before and after slip at varying effective stresses.

on the central part (Figure 2d). The thicknesses of the sheared layers in both clay-rich and calcite-rich samples are uneven, indicating the formation of a poorly sorted fault gouge with wide grain size distribution. The maximum reduction of asperity elevation during slip is about 0.5 mm. The most significant topographic changes happen at high points (peaks), where asperities are believed to be abraded during slip, while low points (valleys) particularly in the shadow of high points remain almost unchanged. The surface roughness coefficient Z_2 decreases from 0.26 to 0.15 for the fault in the clay-rich sample and from 0.24 to 0.13 for the fault in the calcite-rich sample during slip.

3.2. Permeability Changes of Slowly Slipping Faults

The results of shear flow experiments are illustrated in Figure 3 and listed in tables given in the supporting information. The VFT suite of experiments shows that fault permeabilities decline as effective stress increases from 2.5 MPa in Step 1 to 7.5 MPa in Step 2 to 17.5 MPa in Step 3. When effective stress returns to 2.5 MPa in

Step 4, the permeabilities of the saw cut faults fully recover, which we believe is due to the elastic deformation of asperity contacts. In contrast, the permeabilities of the natural faults only partially recover, which is likely due to the compaction of weak and naturally mismatched asperity contacts (Zhao, 1997). The first slip event (Step 5) enhances the permeabilities of both saw cut and natural faults. We interpret that the permeability enhancement is due to additional fluid flow pathways being created by the damage of asperity contacts, as shown in Figure 2. Subsequently, we repeat the above four steps and observe that permeabilities drop with increasing effective stress from Steps 6 to 8 and recover when effective stress returns to 2.5 MPa in Step 9. The reproducibility of permeability results indicates that our assumptions of flow pathways and cross-sectional areas of the fault planes are valid. In the following steps, at a constant effective stress of 2.5 MPa, the permeabilities of the saw cut faults successively increase after each slip event, which is consistent with the fact that produced gouge aligns along the shear direction (Figures 2a and 2b) and serves as newly formed pathways for fluid transport. Although the permeability of the natural fault in the clay-rich sample increases after the second slip event (Step 10), it decreases after additional slip events (Steps 12 and 14). The permeability of the natural fault in the calcite-rich sample continuously decreases after additional slip events (Steps 10, 12, and 14). We interpret that the damage of asperity contacts after the first and/or second slip events may create additional fluid flow pathways. However, the sheared layers shown in Figures 2c and 2d indicate that randomly distributed gouge on the natural faults may not effectively provide fluid flow pathways and likely induces the permeability reduction after a few slip events.

In the VES suite of experiments, we investigate the permeability evolution of the saw cut fault in the clay-rich sample at different effective stresses. The fault permeability slightly increases after the first slip event (Step 2) at 2.5 MPa effective stress but decreases after additional slip events (Steps 5 and 8) at 5.0 and 7.5 MPa effective stresses. We believe that the shear dilation of produced gouge induces the permeability enhancement at low effective stresses, while the gouge compaction blocks fluid flow pathways and leads to the permeability reduction at high effective stresses. This observation is consistent with previous efforts on the permeability change of sheared faults under varying stress conditions (e.g., Gutierrez et al., 2000).

4. Discussion

The poroelastic analysis of simulated faults helps us understand changes in pore space connectivity and pore throat compressibility after slow slip. Previous studies have characterized the permeability of faulted rocks as a function of confining and pore pressures based on an effective pressure law (e.g., Zoback & Byerlee, 1975). Efforts have been subsequently made to understand the stress-dependent permeability of faulted rocks and predict the permeability of such rocks at various effective stresses. The stress-dependent permeability, k , is well described by an exponential function:

$$k(\sigma_{\text{eff}}) = k_0 e^{-c_m \sigma_{\text{eff}}}, \quad (3)$$

where σ_{eff} is the effective stress, k_0 is the intrinsic permeability, and c_m is the stress sensitivity coefficient. We assume that the Terzaghi's principle is valid and the effective stress coefficient is equal to 1; therefore the effective stress is the difference between confining pressure and pore pressure.

Figure 4a shows fault permeability as a function of effective stress before and after the first slip event, obtained from Steps 1–3 and Steps 6–8 in Figure 3, respectively. The logarithmic value of the permeability decreases as effective stress increases, which is in good agreement with an exponential function (equation (3)). The intrinsic permeability is associated with pore throat distribution and pore space connectivity at effective stress equal to zero. The stress sensitivity coefficient is the slope of the exponential curve and reflects pore throat compressibility in cases where changes in tortuosity and connectivity with effective stress can be neglected (Gensterblum et al., 2015). Figure 4b summarizes the intrinsic permeability of each fault before and after the first slip event. The increase in intrinsic permeability of the saw cut fault in the calcite-rich sample is greater than that of the other faults, as the shear layer of this case shows that aligned gouge forms the largest number of fluid flow pathways along the shear direction (Figure 2b). Figure 4c demonstrates that the stress sensitivity coefficient of the saw cut fault in the calcite-rich sample is more sensitive to slip than that of the other faults. This fault is the most compressible because of uniformly distributed asperity changes across the fault plane.

Besides surface roughness and poroelasticity, shale mineralogy also plays an important role in the permeability evolution of sheared faults. Mineralogy strongly affects grain packing in shale faults. A shale fault with high

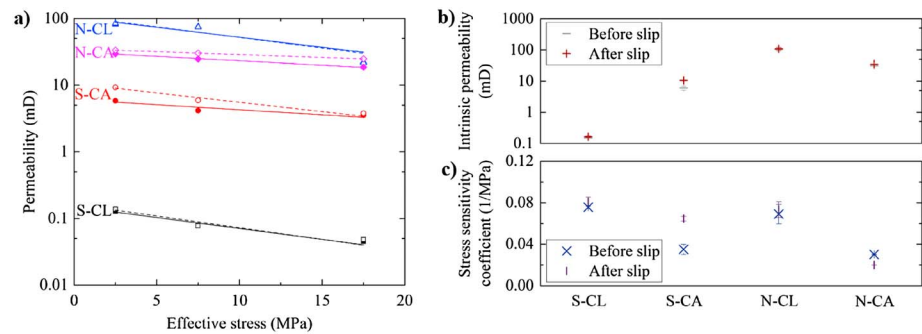


Figure 4. Poroelasticity analysis of saw cut fault in the clay-rich sample (S-CL), saw cut fault in the calcite-rich sample (S-CA), natural fault in the clay-rich sample (N-CL), and natural fault in the calcite-rich sample (N-CA). (a) Permeability as a function of effective stress before (solid lines) and after (dashed lines) the first slip event, (b) intrinsic permeability, and (c) stress sensitivity coefficient for each fault before and after the first slip event, respectively. Error bars in Figures 4b and 4c indicate the 1- σ uncertainty in curve fitting.

calcite content is supported by strong grains with clay fabric partially filling pore space, while a shale fault with high clay content is dominated by clay fabric with strong grains embedded in the matrix (Kohli & Zoback, 2013). During slow slip, strong grains are difficult to comminute but dilate to increase pore space (Bernard et al., 2002), whereas weak clay fabric can smear, bend and break into pieces, and fill pore space (Fang et al., 2017). Our data show that the permeability enhancement during slip of simulated faults with high calcite content is greater than that of simulated faults with high clay content, presumably due to the damage of calcite-rich asperity contacts and slip-associated dilation of strong grains. We believe that the damage of calcite-rich asperity contacts creates additional pathways for fluid flow, and the dilation of strong grains increases pore space in the faults. Nevertheless, clay-rich asperity contacts and produced clay fabric are weak and easily compacted at high stress conditions, resulting in the closure of pore space and the reduction of fault permeability.

Our data suggest that slowly slipping faults have the potential to enhance the permeability of extremely low permeability shale reservoirs at low effective stresses. During hydraulic fracturing, fluid injection reduces effective stress on preexisting faults and induces slow slip (Hubbert & Rubey, 1959), which changes fault surface topography with newly created fluid flow pathways and potentially improves the effectiveness of reservoir stimulation. Particularly, smooth faults with high calcite content could facilitate the recovery of reservoir permeability when effective stress is reduced. Although this study considers fault permeability at low stress conditions, the permeability may be enhanced under other combinations of fault characteristics and stress conditions, motivating further investigations of these coupled processes influencing fault permeability in extremely low permeability reservoirs.

5. Conclusions

We examined fault permeability before and after slow slip to simulate permeability evolution of preexisting fractures and faults in shale reservoirs during hydraulic fracturing. Our results provide important insights into complex permeability patterns controlled by a range of coupled factors, including shale mineralogy, surface topography, and effective stress. Slowly slipping faults at low effective stresses contribute appreciably to permeability enhancement of extremely low permeability shale reservoirs. Smooth fault surfaces and high calcite contents facilitate the recovery of fault permeability when effective stress returns to the initial value. Slowly slipping faults with rough surfaces, in clay-rich rocks, and at higher effective stresses may provide an unfavorable environment for shale gas production from hydraulic fracturing.

References

- Bernard, X. D., Eichhubl, P., & Aydin, A. (2002). Dilation bands: A new form of localized failure in granular media. *Geophysical Research Letters*, 29(24), 2176. <https://doi.org/10.1029/2002GL015966>
- Brace, B. F., Walsh, J. B., & Frangos, W. T. (1968). Permeability of granite under high pressure. *Journal of Geophysical Research*, 73, 2225–2236. <https://doi.org/10.1029/JB073i006p02225>
- Das, I., & Zoback, M. D. (2013). Long-period long-duration seismic events during hydraulic stimulation of shale and tight-gas reservoirs, Part 1: Waveform characteristics. *Geophysics*, 78(6), KS107–KS118. <https://doi.org/10.1190/geo2013-0164.1>

Acknowledgments

We gratefully acknowledge the support of Stanford Center for Carbon Storage and Stanford Rock Physics and Borehole Geophysics Project. Wei Wu was also supported by the Swiss National Science Foundation and the Start-Up Grant from Nanyang Technological University, Singapore. We thank the anonymous reviewers for their thorough review and constructive feedback, which significantly improved the manuscript. The supporting information contains the experimental data presented in the figures.

- Fang, Y., Elsworth, D., Wang, C., Ishibashi, T., & Fitts, J. P. (2017). Frictional stability-permeability relationships for faults in shales. *Journal of Geophysical Research*, *122*, 1760–1776. <https://doi.org/10.1002/2016JB013435>
- Gensterblum, Y., Ghanizadeh, A., Cuss, R. J., Amann-Hildenbrand, A., Krooss, B. M., Clarkson, C. R., ... Zoback, M. (2015). Gas transport and storage capacity in shale gas reservoir—A review, Part: Transport processes. *Journal of Unconventional Oil and Gas Resources*, *12*, 87–122. <https://doi.org/10.1016/j.juogr.2015.08.001>
- Gensterblum, Y., & Zoback, M. D. (2015). Permeability evolution of simulated fractures in unconventional reservoirs with shear displacement and depletion, Stanford Rock Physics & Borehole Geophysics Annual Affiliates Meeting.
- Gutierrez, M., Oino, L. E., & Nygard, R. (2000). Stress dependent permeability of a de-mineralized fracture in shale. *Marine and Petroleum Geology*, *17*(8), 895–907. [https://doi.org/10.1016/s0264-8172\(00\)00027-1](https://doi.org/10.1016/s0264-8172(00)00027-1)
- Heller, R., Vermilyen, J., & Zoback, M. (2014). Experimental investigation of matrix permeability of gas shales. *The American Association of Petroleum Geologists Bulletin*, *98*(5), 975–995. <https://doi.org/10.1306/09231313023>
- Hubbert, M. D., & Rubey, W. W. (1959). Role of fluid pressure in mechanics of overthrust faulting. *Geological Society of America Bulletin*, *70*(2), 115–205. [https://doi.org/10.1130/0016-7606\(1959\)70%5B115:ROFPIM%5D2.0.CO;2](https://doi.org/10.1130/0016-7606(1959)70%5B115:ROFPIM%5D2.0.CO;2)
- Kohli, A. H., & Zoback, M. D. (2013). Frictional properties of shale reservoir rocks. *Journal of Geophysical Research: Solid Earth*, *118*, 5109–5125. <https://doi.org/10.1002/jgrb.50346>
- Lee, H. S., & Cho, T. F. (2002). Hydraulic characteristics of rough fractures in linear flow under normal and shear load. *Rock Mechanics and Rock Engineering*, *35*(4), 299–318. <https://doi.org/10.1007/s00603-002-0028-y>
- Reece, J. S., Zoback, M. D., & Kohli, A. H. (2014). Effect of shear slip on fault permeability in shale reservoir rocks, abstract H13Q-03. Presented at 2014 fall meeting, American Geophysical Union, San Francisco, CA, Dec. 15–19.
- Scheidegger, A. E. (1974). *The physics of flow through porous media* (3rd ed.). Toronto, Canada: University of Toronto Press.
- Sone, H., & Zoback, M. D. (2013a). Mechanical properties of shale-gas reservoir rocks—Part 1: Static and dynamic elastic properties and anisotropy. *Geophysics*, *78*(5), D381–D392. <https://doi.org/10.1190/geo2013-0050.1>
- Sone, H., & Zoback, M. D. (2013b). Mechanical properties of shale-gas reservoir rocks—Part 2: Ductile creep, brittle strength, and their relation to the elastic modulus. *Geophysics*, *78*(5), D393–D402. <https://doi.org/10.1190/geo2013-0051.1>
- Tse, R., & Cruden, D. M. (1979). Estimating joint roughness coefficient. *International Journal of Rock Mechanics and Mining Science and Geomechanics Abstracts*, *16*(5), 303–307. [https://doi.org/10.1016/0148-9062\(79\)90241-9](https://doi.org/10.1016/0148-9062(79)90241-9)
- Zhao, J. (1997). Joint surface matching and shear strength, part A: Joint matching coefficient. *International Journal of Rock Mechanics and Mining Sciences*, *34*(2), 173–178. [https://doi.org/10.1016/S0148-9062\(96\)00062-9](https://doi.org/10.1016/S0148-9062(96)00062-9)
- Zoback, M. D., & Byerlee, J. D. (1975). Permeability and effective stress. *Bulletin of the American Association of Petroleum Geologists*, *59*, 154–158.
- Zoback, M. D., Kohli, A. H., Das, I., & McClure, M. (2012). The importance of slow slip on faults during hydraulic fracturing stimulation of shale gas reservoirs, Americas unconventional resources conference, Pittsburgh, PA, Jun. 5–7.